Published in "*Soil water repellency: occurrence, consequences and amelioration*", Elsevier, 2002, Ch. 23.

Non-equilibrium Model for Gravity-Driven Fingering in Water Repellent Soils: Formulation and 2-D Simulations

J. Nieber[†], A. Sheshukov[†], A. Egorov[‡] and R. Dautov[‡]

[†] Biosystems and Agricultural Engineering Department and Army High Performance Computing Research Center, University of Minnesota, 1390 Eckles Avenue, Saint Paul, MN 55108, U.S.A.

[‡] Kazan State University, Universitetskaya 17, Kazan 420008, Russia

Abstract

The instability of infiltrating flow is studied using the mass balance equation coupled with a first-order relaxation equation relating the rate of change of saturation to the difference between the dynamic water pressure and the saturation-dependent equilibrium water pressure. A numerical solution of the mass balance equation, based on a mass conservative scheme, is applied to the simulation of infiltrating flows in a vertical, two-dimensional plane region. Both water wettable and water repellent soils are considered in the analysis. The effect of water repellency is introduced by modification of the equilibrium saturation - pressure relationship, in which water repellency causes the relation to become flatter. Conditions of even slight water repellency are found to be sufficient to cause infiltrating flows to become unstable. A sensitivity analysis related to the width of the surface source shows that the number of fingers generated increases with increasing source width. The sensitivity analysis also indicates that the non-equilibrium model approach can provide a physically plausible reason for flows becoming stable when the surface flux becomes vanishingly small.

1 Introduction

Preferential flow of water in soils impacts several soil attributes, including the capacity of soils to remove/treat harmful constituents, and the capacity of soils to provide water and nutrients to plants. Nieber (2000) describes the several recognized forms of preferential flow, among these being the process of gravity-driven unstable flow. The earliest reported observations of gravity-driven unstable flow were reported by Hill (1952) in a study of flow in chemical separation columns. At the present time there is still much interest in experimental and theoretical descriptions of gravity-unstable flow.

As described by Raats (1973), the process of gravity-driven unstable flow may occur when the following conditions are met: 1) the saturated hydraulic conductivity increases with depth; 2) the soil is water repellent; 3) air pressure builds up at the wetting front of infiltrating water. In addition to the conditions, recent analyses by Egorov et al. (2002) show that the conditions for instability of flow requires that non-equilibrium in the saturation - pressure relation exist. For all of these conditions, the wetting front slows and the front becomes unstable, manifested by the breaking of the front into discrete fingers.

Several mathematical models have been developed to quantify the conditions for flow instability in soils (Raats, 1973; Philip, 1975; Parlange and Hill, 1976, Diment et al., 1982; Glass et al., 1989). Most of these studies have provided a means to estimate finger width, but none of them dealt directly with the mechanism of finger formation. It is now recognized (Dautov et al., 2002) that there are two requirements for the successful modeling of finger formation. These requirements are that (i) the mathematical model must be capable of producing unstable perturbations and (ii) the growing perturbations have to be persistent. The numerical model presented by Nieber (1996, 2000) and Ritsema et al. (1998) correctly incorporated the means for the persistence of fingers by using capillary hysteresis in the water retention function. That numerical model however was deficient in the method for the formation of flow instabilities, because it was based on the solution of the Richards equation, which is now understood to be unconditionally stable (Otto, 1997; Egorov et al., 2002).

In the work by Egorov et al. (2002), the conditions for growth of infinitesimal perturbations imposed on a uniform wetting front are well quantified. They analyzed three possible mathematical models: the conventional Richards equation, a sharp front Richards equation (Selker et al., 1992), and an extended

Richards equation with a non-equilibrium saturation - pressure function (Hassanizadeh and Gray, 1993). They showed that the conventional Richards equation is unconditionally stable, while the sharp-front Richards equation is unconditionally unstable and yields an unstructured field of fingers. The conclusion was that neither of these models should be used to describe fingering. The non-equilibrium Richards equation model was found to be the only model capable of generating a structured field of fingers from a slightly perturbed uniform wetting flow. In a subsequent paper, Dautov et al. (2002) applied this non-equilibrium model to simulate single and multiple fingers in water wettable soils. Hysteresis in the saturation - pressure relation was incorporated in the model to provide persistence of the growing fingers.

Raats (1973) listed soil water repellency as one of the possible causes of gravity-driven unstable flows in soils. This has been confirmed experimentally by numerous research articles including Jamison (1945), Hendrickx et al. (1993), Ritsema et al. (1993), Ritsema and Dekker (1994), and Dekker and Ritsema (1996). Modeling of unstable flow in water repellent soils has been reported by van Dam et al. (1990), de Rooij (1995), de Rooij and de Vries (1996), Ritsema et al. (1998), Nguyen et al. (1999), and Nieber et al. (2000).

In this manuscript we formulate a non-equilibrium model for flow in unsaturated porous media, and present a numerical solution scheme to solve the governing equations. This numerical solution is then applied to the simulation of two-dimensional flow in unsaturated soils. The conditions considered are for a well-graded sand that is either completely water wettable or slightly water repellent. It is shown that the condition of complete water wettability leads to a stable flow, while the slight water repellency leads to instability and persistent finger formation. The sand media studied by Bauters et al. (2000) and Nieber et al. (2000) is used as a guide for quantifying the impact of water repellency on the saturation – pressure relationship of the porous medium.

2 Model formulation

Unsaturated flow in porous media is conventionally modeled using the Richards equation when the air phase is assumed to be at ambient atmospheric pressure. This equation may be written in dimensionless form as

$$\frac{\partial s}{\partial t} - \nabla \cdot K(s)\nabla p + \frac{\partial}{\partial z}K(s) = 0 \tag{1}$$

$$p = \mathrm{P}(s) \tag{2}$$

where s is the effective saturation ($0 \le s \le 1$), p is the water pressure, K is the relative hydraulic conductivity, $\mathrm{P}(s)$ is the equilibrium pressure represented by the relationship between saturation and water pressure, and z is the vertical coordinate taken positive downward. The pressure and the spatial coordinates are normalized on air-entry pressure taken as $1/\alpha$, the relative hydraulic conductivity is normalized on its saturated value, K_s, and time is scaled on $\phi(1-s_r)/(\alpha K_s)$, where ϕ is the porosity, α is the well-known van Genuchten (1980) parameter, and s_r is the residual saturation. The system (1) and (2) is completed by defining the hydraulic properties of the porous medium. In this paper we adopt the van Genuchten-Mualem model (van Genuchten, 1980), which may be expressed in the non-dimensional form as

$$\mathrm{P}(s) = -\left(s^{-1/m} - 1\right)^{1/n}, \quad K(s) = s^{1/2}\left(1 - \left(1 - s^{1/m}\right)^m\right)^2, \quad m = 1 - \frac{1}{n} \tag{3}$$

The recent results by Egorov et al. (2002) and Otto (1997) proved that any solution of the Richards equation is unconditionally stable. Therefore, the conventional model must be modified to be able to describe fingering phenomena in unsaturated porous media. Hassanizadeh and Gray (1993) suggested one possible extension of the Richards equation. This model takes into account dynamic memory effects by adding a mechanism of relaxation in the relation between water saturation and water pressure. The non-equilibrium mechanism of relaxation is manifest in the results of several experimental studies including Nielsen et al. (1962), Topp et al. (1967), Smiles et al. (1971) and Wildenschild et al. (2001). The non-equilibrium model does not change equation (1), but replaces the relationship (2) with

$$\tau \frac{\partial s}{\partial t} = p - \mathrm{P}(s) \tag{4}$$

where $\tau > 0$ denotes the dimensionless relaxation coefficient function. The dimensional relaxation coefficient (m sec) is normalized on $\phi/\left(\alpha^2 K_s\right)$. Note that in general $\mathrm{P}(s)$ can be hysteretic and, therefore, two main hysteretic curves: $p = \mathrm{P}_w(s)$ (main wetting curve or MWC) and $p = \mathrm{P}_d(s)$ (main drainage curve or MDC), are incorporated in the model. These two curves divide the (p,s)-plane into three domains: the main hysteretic loop H_0, the domain H_w above the MWC, and the domain H_d below the MDC (Figure 1). This hysteretic non-equilibrium model postulates (Beliaev and Hassanizadeh, 2001) that dynamic memory effects (relaxation) are significant only outside the main hysteretic loop, and it takes those effects into account using the same modification of the saturation - pressure relation as in equation (4) . The relaxation equation is therefore given by

$$\tau_i \frac{\partial s}{\partial t} \equiv \tau_i \dot{s} = p - \mathrm{P}_i(s), \qquad (p,s) \in H_i, \quad i = w,d \tag{5}$$

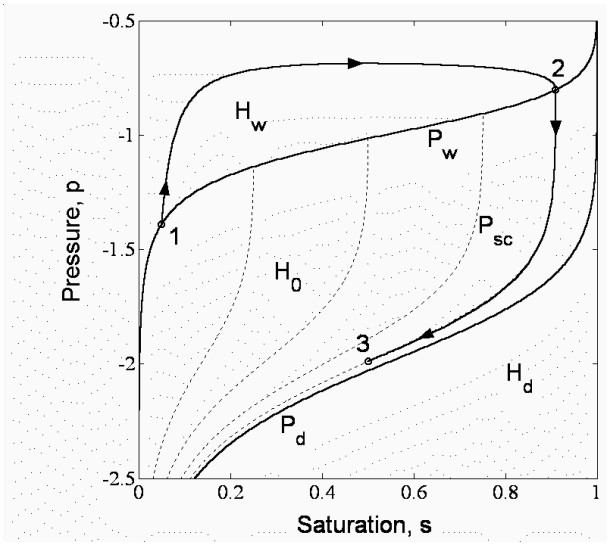

Figure 1 A typical closed-loop hysteresis diagram. The dashed lines represent the scanning drainage curves. The trajectory of the process follows points 1 (initial state), 2 (switching point), and 3 (final state).

As a result of this postulate it is assumed that inside the main hysteretic loop region H_0, wetting/drainage processes follow equilibrium scanning curves. In this paper we use the hysteresis model of Mualem (1974) and restrict our attention only to the two-stage wetting-drainage process. Trajectories for the wetting stage locate within H_w, while trajectories for the drainage stage will be limited to H_0. The non-equilibrium drainage domain H_d will never be visited for this two-stage process. As a result of the applied conditions scanning curves turn out to be the primary drainage scanning curves (Mualem, 1974), yielding the relations

$$p = \mathrm{P}_{sc}(s, s_*) \quad \text{or} \quad s = \mathrm{S}_{sc}(p, s_*) \quad \text{for} \quad (p,s) \in H_0 \tag{6}$$

$$\mathrm{S}_{sc}(p, s_*) = \mathrm{S}_w(p) + \frac{s_* - \mathrm{S}_w(p)}{1 - \mathrm{S}_w(p)} \left(\mathrm{S}_d(p) - \mathrm{S}_w(p)\right) \tag{7}$$

where S_{sc}, S_w, and S_d are the inverse functions of P_{sc}, P_w, and P_d respectively, and s_* corresponds to the switching point (point 2 in Figure 1).

Equations (5) and (6) may be transformed to one equation by introducing the continuously differentiable functions $p = \mathrm{P}_t(s)$ and $s = \mathrm{S}_t(p)$:

$$\mathrm{P}_t(s) = \begin{cases} \mathrm{P}_w(s(t)), & \dot{s} \geq 0 \\ \mathrm{P}_{sc}(s(t), s_*), & \dot{s} < 0 \end{cases}, \qquad \mathrm{S}_t(s) = \begin{cases} \mathrm{S}_w(p(t)), & \dot{p} \geq 0 \\ \mathrm{S}_{sc}(p(t), p_*), & \dot{p} < 0 \end{cases}$$

where $s_* = \max s(t)$, and $p_* = P_w(s_*)$. With these definitions the saturation - pressure relations given by equations (5) and (6) may be rewritten in terms of P_t as

$$\tau \dot{s} = p - \mathrm{P}_t(s), \quad \tau = \begin{cases} \tau_w, & (p,s) \in H_w \\ 0, & (p,s) \in H_0 \end{cases}$$

For this paper we have adopted the functional form for τ_w given by

$$\tau_w = \tau^0(s)\left(p_0 - p\right)_+^\gamma, \quad \tau^0(s) = \tau_s^0 \, \mathrm{P}_w'(s), \quad \gamma > 0 \tag{8}$$

where $(\cdot)_+ = \max(\cdot, 0)$, p_0 is the parameter referred to as the water entry pressure of the soil (Baker and Hillel, 1990; Selker et al., 1992), and τ_s^0 is the relaxation constant. The function $\tau_s^0 \, \mathrm{P}_w'(s)$ is unbounded at saturations approaching zero and unity. The selection of this form for the function is based on the homogenization analysis of Panfilov (1998) in his study of two-phase flow in double porosity media. The use of the term $\left(p_0 - p\right)_+^\gamma$ imposes a limit on the growth of pressure during flow. Without this term the traveling wave solution presented by Egorov et al. (2002) yields non-physical behavior in the form of an unbounded pressure, as the initial saturation approaches zero. For more detailed information on the selection of equation (8) to represent the dimensionless relaxation time the reader is referred to Dautov et al. (2002).

With the functional form for $\tau^0(s)$ given in equation (8) we finally have for the relaxation equation

$$\tau \dot{\mathrm{P}}_t = p - \mathrm{P}_t(s) \tag{9}$$

where the relaxation coefficient is now defined as $\tau = \tau_s^0 \left(p_0 - p\right)_+^\gamma$, and $\tau_s^0 = 0$ inside H_0. Note that in the actual numerical implementation of this approach, rather than setting $\tau_s^0 = 0$ inside H_0, it is set to a small constant $\simeq 10^{-3}$. Using this small value serves to allow the description of processes inside and outside the main hysteretic loop by the same procedure, thus facilitating the use of the same algorithm in all computations.

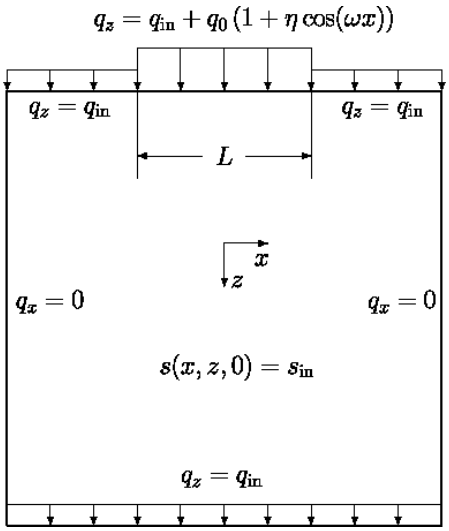

Figure 2 Schematic of the computational domain with specified initial and boundary conditions.

The system of equations (1) and (9) is subject to the initial and boundary conditions that are shown in Figure 2. They are

$$t = 0: \quad s = s_{in} \tag{10}$$

$$z = 0,\ x_l \le x \le x_r: \quad q_z = q_{in} + q_0 \int_{x_a}^{x_b} \left(1 + \eta\cos(\omega\xi)\right)\delta(\xi - x)\,dx \tag{11}$$

$$z = z_d: \quad q_z = q_{in} = K(s_{in}) \tag{12}$$

$$x = x_l \quad \text{and} \quad x = x_r: \quad q_x = 0 \tag{13}$$

where δ is the Dirac function, x_l, x_r, and z_d are the left, right and lower boundaries of the computational domain, while x_a, x_b, and $L = x_b - x_a$ are the boundaries and the length of the infiltration source. By equation (11) the infiltration flux q_0 is perturbed with a sinusoidal function having amplitude η and frequency ω. To assure that the process studied is a two-stage wetting-drainage process, we maintain the uniform gravity-driven background flux q_{in} related to the initial saturation s_{in} over both the lower boundary and the portion of the upper boundary outside of the infiltration source. The implementation of the condition given by equation (12) is valid until the infiltrating front reaches the bottom boundary.

3 Discretization and numerical solution

The system of equations (1) and (9) with initial and boundary conditions (10)–(13) is solved numerically by applying a mass-conservative finite difference approximation and evaluating the temporal terms by a fully implicit first-order backward Euler scheme. Details of this numerical solution scheme are presented in Dautov et al. (2002). The resulting nonlinear algebraic equations may be written in matrix form as,

$$\begin{aligned} &\frac{s-\tilde{s}}{\Delta t} + A(s)H = 0, \qquad p = H + Z \\ &\tau(p,s)\frac{\mathrm{P}-\tilde{\mathrm{P}}}{\Delta t} = p - \mathrm{P}, \qquad s = \mathrm{S}_t(\mathrm{P}) \end{aligned} \tag{14}$$

where *s*, *p*, and *H* are the unknown vectors of nodal values of saturation, pressure, and hydraulic head fields respectively, *A* is the symmetric 5-diagonal matrix with coefficients dependent on *s*, $\tau(p,s)$ is a diagonal matrix, and *tilde* indicates values at the previous time-step. Note that the hydraulic head variable has been substituted into equation (1) to arrive at equation (14). The advantage of using the hydraulic head variable instead of the pressure head variable in the mass balance equation is that the convective term (third term in equation (1) resulting from gravity) causes some numerical dispersion. The use of the hydraulic head variable eliminates this source of numerical dispersion.

The set of nonlinear algebraic equations given by equation (14) are solved by the following iteration procedure. Here *k*+1 indicates the current iteration level.

1) Let $k = 0$, and set $p^k = \tilde{p}$, $s^k = \tilde{s}$, $H^k = \tilde{p} - Z$

2) Find P^{k+1} and s^{k+1} from the explicit relations

$$\tau(p^k, s^k)\frac{\mathrm{P}^{k+1}-\tilde{\mathrm{P}}}{\Delta t} = p^k - \mathrm{P}^{k+1}, \quad s^{k+1} = \mathrm{S}_t(\mathrm{P}^{k+1})$$

3) Solve the linear system of algebraic equations for H

$$A(s^{k+1})H^{k+1} + D^{k+1}H^{k+1} = D^{k+1}H^k - \frac{s^{k+1}-\tilde{s}}{\Delta t} \tag{15}$$

The diagonal matrix D^{k+1} is the approximation of the derivative of the vector-valued function $(s-\tilde{s})/\Delta t$ with respect to *p*:

$$D^{k+1} = \frac{\mathrm{S}_t'(\mathrm{P}^{k+1})}{\Delta t}\frac{d}{dp}\left(\frac{p\Delta t + \tau(p,s^{k+1})\tilde{\mathrm{P}}}{\tau(p,s^{k+1}) + \Delta t}\right)\Bigg|_{p=p^k}$$

Upon solving for H, the pressure is calculated as $p^{k+1} = H^{k+1} + Z$.

4) Set $k = k+1$, and go to step 2). Repeat the loop until convergence is reached.

To obtain the solution for H^{k+1} we invert the matrix of the system (15) using a preconditioned conjugate gradient method based on modified incomplete Cholesky factorization. We note that the resulting matrix $A(s^{k+1}) + D^{k+1}$ of the system has good algebraic properties: it is symmetric, 5-diagonal, and positive definite.

Within the iteration loop 1)-4) the hysteretic state at a particular grid point is not changed, but instead iteration continues until absolute and relative errors in pressure and saturation between two consecutive iterations is less than a value ε. The change in hysteretic state is checked after convergence. To assess whether any saturation reversals have occurred at the end of each time step, we check for changes in the nodal saturations from the previous time step. If the sign of $s_{i,j} - \tilde{s}_{i,j}$ at a node (i, j) has changed, and $\left|s_{i,j} - \tilde{s}_{i,j}\right| > 10\varepsilon$, the hysteretic state for the node is changed.

Our experience with this numerical solution has been very positive. We have found that the solutions are achieved very efficiently. For the two-dimensional problems solved here all of the solutions were performed on an 800 MHz Pentium III PC. Grid sizes were upwards of 20,301 nodes. All solutions were achieved within one-half hour run time.

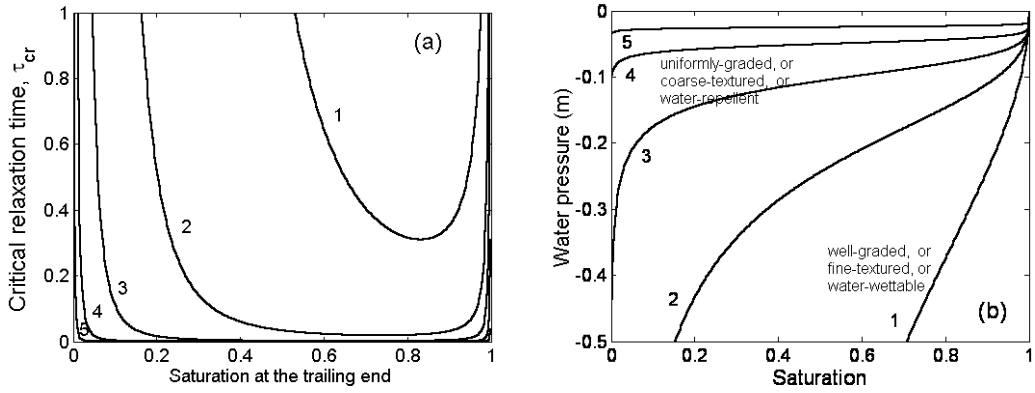

Figure 3 (a) Critical dimensionless relaxation time versus saturation at the trailing end of an advancing wetting front, and (b) Equilibrium saturation - pressure relationships for distinct n and α: 1 - $n = 2, \alpha = 2$; 2 - $n = 3, \alpha = 5$; 3 - $n = 5, \alpha = 10$; 4 - $n = 10, \alpha = 20$; and 5 - $n = 20, \alpha = 40$.

4 Conditions leading to unstable flows

Based on the use of a traveling wave solution to equations (1) and (9), Egorov et al. (2002) showed that unstable flow occurs when the relaxation parameter τ is sufficiently large. Unstable flows are manifested by a non-monotonic distribution of saturation in the direction of the flow. Egorov et al. showed that it is possible for the relaxation parameter to be just large enough to produce a stable flow with a slightly non-monotonic saturation profile. However, for a value greater than a quantifiable critical value, τ_{cr}, the non-monotonic flow will be unstable.

A plot of the critical dimensionless relaxation time τ_{cr} and the degree of saturation at the trailing end of an advancing wetting front is shown in Figure 3a. The plotted lines were derived for various values of van Genuchten parameters α and *n*. The corresponding retention curves derived from the van Genuchten equations are shown in Figure 3b. Coarse textured soils, including sands and gravels, will tend to have values of *n* exceeding 3. Soils with narrow particle size distributions will also tend to have larger values of *n*. In contrast, fine textured soils and well-graded soils, will tend to have smaller values of *n*, in the range of 1.1 to 2.5.

The lines plotted in Figure 3a show that for either low or high trailing saturations, the flow is likely to be stable because the critical value of τ increases without bound as the trailing saturation approaches zero or unity. But in the range of trailing saturations between about 0.2 and 0.9, the flow is more likely to become unstable because the critical value of τ is a minimum in that saturation range.

The dependence of τ_{cr} on the value of the van Genuchten *n* is instructive with respect to the type of soil/porous medium that will promote unstable flows. The plots in Figure 3a show that as the value of *n* increases, the function $\tau_{cr}(s)$ decreases, leading to an increasing range of saturations over which instability will be possible. Referring to corresponding curves in Figure 3b, we may conclude that coarser textured soils, and soils with narrow particle size distributions will tend to support unstable flows.

To put the values on the plot in Figure 3a into perspective, Hassanizadeh (1997) indicated that the dimensionless relaxation time likely ranges between 1 and 2000 for sandy soils. Comparing this range to the plots in Figure 3a indicates that flows in sandy soils should tend to be unstable over a fairly large range of saturations. Typical values of dimensionless relaxation time are not available for fine texture soils, but current theory (Baliaev and Hassanizadeh, 2001) indicates that the values should be larger than those for sandy soils. Since fine textured soils will have smaller values of *n*, it is necessary to have a much larger value of relaxation time to produce instability. So while non-equilibria may be a feature common to all soils, it may not lead to instability.

The above analysis will be applied in the following sections to explain why water repellency in a soil can cause flows in the soil to become unstable.

5 Simulation results

The mathematical model and the numerical method derived in the preceding sections may be applied to study fingering in soils that exhibit significant non-equilibrium in the saturation - pressure relation. Fingering has been observed to occur in initially dry uniformly graded soils (Hill and Parlange, 1972; Glass et al., 1989), while it does not tend to be manifested in well-graded wettable soils or initially moist soils (Liu et al., 1994). Fingering has also been observed in well-graded water repellent soils (Ritsema and Dekker, 1994; Bauters et al., 2000). We hypothesize that the manifestation of fingering is related to the presence of at least the critical amount of non-equilibria in the saturation - pressure relation. At present there does not exist sufficient experimental measurements of dynamic saturation - pressure relations to determine whether this hypothesis is correct, so for now we will use a rational approach to quantify the degree of non-equilibrium of the saturation - pressure relation.

Our rational analysis is based on the relaxation model given by equation (9), and we rely on the support of the experimental studies presented by Bauters et al. (2000). The sand used in the experiments was fairly well-graded as described by Nieber et al. (2000). The saturation – pressure curves shown by Bauters et al. show that the degree of water repellency is strongly manifested in the wetting curves, while little effect is observed in the drainage curves. The wetting curve for the water wettable sand manifested characteristics of a fairly well-graded sand, but as the degree of water repellency increased, the wetting curves exhibited the flatter saturation – pressure curve characteristics of uniformly graded porous media. Also, as the degree of repellency increased, they found that the water entry pressure increased to zero and then became positive for the cases of highest water repellency.

For this manuscript we will examine the effect of flatness of the saturation – pressure relationship on the stability of infiltrating flows. Based on experimental evidence of Bauters et al. (2000), we conclude that as a porous medium becomes more water repellent, the corresponding saturation – pressure relationship becomes flatter. The flattening of the saturation – pressure relationship is quantified by an increase in the van Genuchten *n* parameter. According to the analysis presented in the previous section, the flatter the saturation – pressure curve, and thereby the larger the value of *n*, the more likely is the transition from a stable flow to an unstable flow.

We are interested to determine the effect of saturation - pressure parameters on flow stability. This effect will be demonstrated by examining the flow from a point source. Through this example we will show that for sufficiently large dimensionless relaxation time coefficient, the flow will lead to a defined finger, while for smaller values the flow will be stable. After demonstrating this effect we will consider the generation and propagation of multiple fingers from a finite surface source, and we will show that the number of fingers generated depends on the width of the source.

We note here that a sharp-front regime may occur for some range of the input parameters (i.e., very dry soils), and very fine grids are required to adequately simulate a steep change in saturation over the front. We designed the grids so that the sharp fronts would be represented by at least four nodes. With this in mind the input parameters used in the calculations were taken within a range that allowed us to deal with reasonable grids of less than 25,000 nodes.

To specify the hysteretic non-equilibrium model, it is necessary to define the hydraulic properties of the medium such as $K(s)$, $\mathrm{P}_w(s)$ and $\mathrm{P}_d(s)$, as well as τ_w as a function of parameters of the process. We used the van Genuchten-Mualem relationships given by equation (3), and specified the dimensionless inverse capillary length $1/\alpha_d = 2/\alpha_w$, and pore-size distribution parameter $n_w = n_d$. We will present results only for the case with $\gamma = 1$ and $\varepsilon = 10^{-7}$ since varying these parameters over a reasonable range

while keeping the other parameters constant led to qualitatively similar behavior for all simulations. Parameters n and τ_s^0 are varied in the calculations to show the impact of the dimensionless relaxation time on stability.

5.1 Single finger from a narrow surface source

The single finger is generated by infiltration over a small length L at the upper boundary with the flux $q_0 > 0$. The applied flux at the soil surface shown in Figure 2 is less than the saturated hydraulic conductivity so that $q_0 < 1$. The parameters for the simulation were chosen to be, $\tau_s^0 = 5$, $q_0 = 0.2$, $L = 1$ and $s_{in} = 0.075$. The total flux is then $Q = q_0 L = 0.2$. Since we expected only a single finger to form, the grid was refined horizontally in a vertical column in the vicinity beneath the location of the source. There the horizontal grid cell dimension was 2/3 of the dimension in the region outside the refined zone. The total grid was composed of 91 cells horizontally and 151 cells vertically.

The saturation and pressure head distributions at $t = 106$ are illustrated in Figure 4. The saturation distribution is represented as a clearly defined finger. The width of this finger is determined by the flux Q.

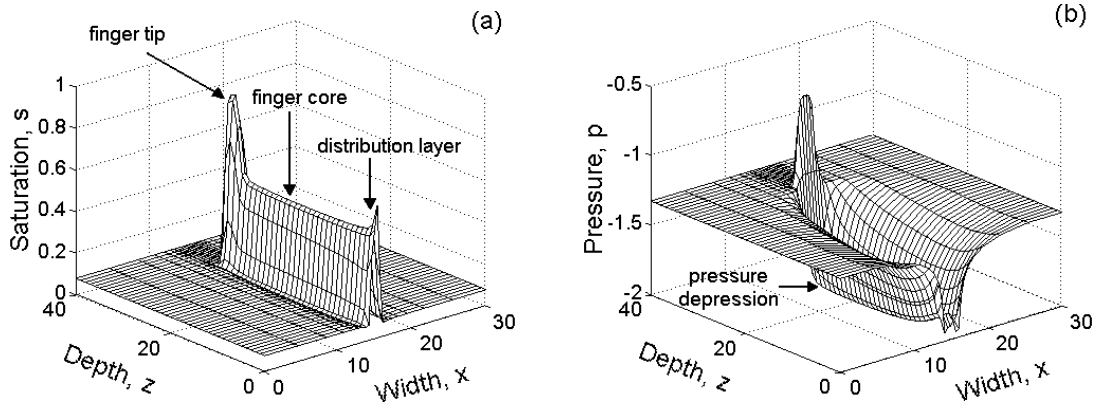

Figure 4 Saturation (a) and pressure head (b) distribution for the case of a single finger: $n = 10, \tau_s^0 = 5, L = 1, q_0 = 0.2$, and $s_{in} = 0.075$.

The morphology of the finger is defined by three distinct features. First, as illustrated in Figure 4a the finger tip has a higher water saturation, stationary finger core and a distribution layer (Ritsema and Dekker, 1994). Second, once developed the distribution layer remains steady while the tip of the finger moves at a constant velocity without change in shape and the finger core length grows at a steady rate. Third, lateral spreading of the finger core is halted by the pressure inside the finger being smaller than the background pressure as shown in Figure 4b. We emphasize that the main characteristics of the finger are uniquely designated by Q. For other simulation runs we performed we found that by imposing different values of Q the finger velocity, finger width, and saturation at both the tip of the finger and the finger core increase with Q. This scenario is fully consistent with the physical picture of the process presented by Liu et al. (1994) and Nieber (1996).

The distribution layer provides a steady water flux into the finger core. For the case of a narrow source shown in Figure 4 the distribution layer is quite narrow. In Figure 4a the distribution layer is identifiable by the higher saturation near the source location.

The influence of water repellency of the soil on finger size is illustrated in Figure 5 which shows the position of the $s = 0.1$ isoline at $t = 106$ for various values of the parameters n and τ_s^0. Plots of the saturation profile along the central axis of the domain are shown in Figure 6a, while pressure head profiles along the same central axis are shown in Figure 6b.

Curves 1 and 3 are for a solution with very small τ_s^0 and therefore represent the solution to the conventional Richards equation. For both of these cases the flow is diffuse even though increasing n reduces the lateral diffusion and makes the saturation profile steeper at the wetting front. However, there is

no accumulation of water at the front and this coincides with the conventional theory described by the Richards equation.

Curves 2, 4 and 5 represent the solution where the non-equilibrium mechanism is included in conjunction with hysteresis in the saturation - pressure relation. For these cases the flow shows different degrees of non-monotonicity in the saturation profile. For case 2 the degree of non-monotonicity is only slight, and for this case the flow is stable. For cases 4 and 5 the degree of non-monotonicity is significant and the flow profile has all the characteristics of finger flow. It is interesting to note that while case 2 has the same value of τ_s^0 as cases 4 and 5, the small value of *n* in the first case causes the flow to be stable, while the larger value for the latter two cases leads to unstable flow. This comparison points to the importance of the shape of the saturation - pressure function on flow stability. A soil having a saturation – pressure function with relatively small *n*, even if the value of τ_s^0 is large, will not support unstable flows. In contrast, soils with large values of *n* will support unstable flows.

The effect of water repellency on the formation of unstable flows can be directly assessed by comparison of case 2 and cases 4, 5. While for all three cases the value of τ_s^0 is the same, the value of n is very different among the three cases. In reference to the water repellent treatments described by Bauters et al. (2000), we might look at case 2 as representing the water wettable sand, while cases 4 and 5 represent the same sand but with increasing levels of water repellency.

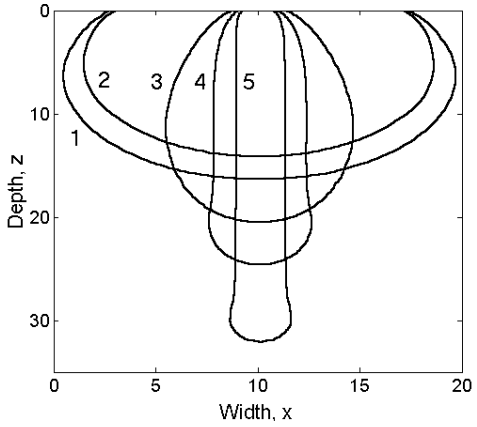

Figure 5 Saturation isolines s=0.1 represented a finger size for $q_0 = 0.2, L = 1, s_{in} = 0.075$ and five distinct cases: 1 – $n = 2, \tau_s^0 = 0$; 2 – $n = 2, \tau_s^0 = 5$; 3 - $n = 5, \tau_s^0 = 0$; 4 - $n = 5, \tau_s^0 = 5$; and 5 – $n = 10, \tau_s^0 = 5$.

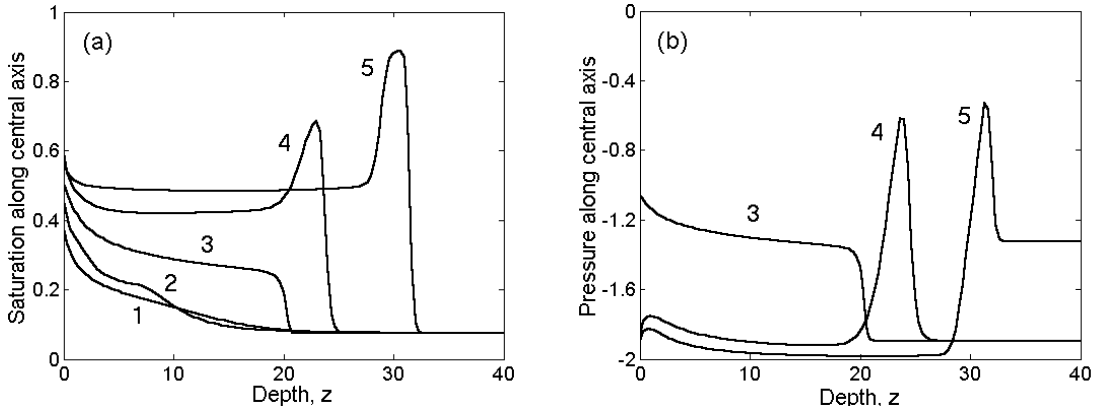

Figure 6 (a) Saturation and (b) pressure head along the central vertical line $x = 10$ for the five cases presented in Figure 5. The pressure head profiles are not shown for cases 1 and 2 because they both plot below the line of pressure head equal to –2.

5.2 Multiple fingers from a finite surface source.

In the previous section we demonstrated the apparent effect of water repellency on the saturation – pressure relationship and showed that this can lead to instability of gravity-driven flow. In the present section we will confine our analysis to the case of unstable flow only and focus on the effect of source width on finger number and finger velocity. For this analysis the following parameters are used: $n = 7$, $\tau_s^0 = 5$. These are parameters that we know will produce wetting front instability.

We will now show that by increasing the length L of the infiltration source an increasing number of fingers will form. The width and velocity of individual fingers will be shown to be affected by the length L. Two sets of conditions will be considered. In the first set we will keep the total applied flux Q constant while varying L. Thus as L increases, the surface flux intensity $q_0 (Q/L)$ will decrease. The value of Q was set to 0.5 for this set. For the second set we will keep q_0 constant as L is varied leading to increasing Q with increasing L. The value of q_0 is set to 0.2 for this set.

For all of these simulation runs the width of the region was 50 and covered by a uniform grid. For the first set the length of the flow region was 100, and covered by a grid of 101 by 201 cells. For the second set the length was 60, with a grid of 101 by 121.

The initial condition for the flow domain is the same as that applied for the case of a single finger generated from a point source described in the last section. In this case however, we apply a high-frequency, low-amplitude sinusoidal perturbation ($\eta \sim 10^{-2}$) to the surface flux. This perturbed flux is described by equation (11). The small gravity-driven background flux is again applied to ensure that the flow is maintained as a two-stage process. The initial saturation s_{in} for the first set was set to 0.075, while it was set to 0.1 for the second set of runs.

5.2.1 Constant total flux with varying source width

The analysis of the case of a constant total flux with varying source width is considered first. The numerical solution results are displayed in Figure 7 for four cases of source width. For the case of $L = 1$, essentially the case of a point source at the surface, we get a single finger. The plot in Figure 7a shows the single finger at a time of 210. For this value of L there is no obvious distribution layer because the finger has larger width than the width of the source at the surface. The finger has a high saturation at the tip of the finger, and the saturation decreases monotonically behind the finger tip.

For the case of the source width with $L = 10$, the initial source breaks into two fingers at a depth of $z \simeq 7$ as shown in Figure 7b. The flow into the single finger for $L = 1$ is equal to $Q = 0.5$, while the flow into each of the two fingers in Figure 7b is approximately equal to $Q = 0.25$ since the total flux at the surface is approximately split equally between the two fingers. The plot in Figure 7b shows the position of the fingers at a time of 288, about 30% longer time than for that shown in Figure 7a. While the position is about the same as shown in Figure 7a, the time is longer because the flow in the fingers in this second case is smaller. This result shows that the finger velocity is related to the flux in the finger.

When the width of the surface source is set to $L = 20$ the flow breaks into three fingers. The fingers on the left and the right side of the formation first formed when the distribution layer was at a depth of $z \simeq 12$. With time the distribution layer moved downward between these two fingers and a third finger formed at a depth of $z \simeq 22$. The flux in the two outside fingers is about equal, while the flux within the middle finger is somewhat higher. This difference in flux explains why the position of the middle finger is about the same with the other two fingers at $t = 375$. This difference also shows why the core of the middle finger appears to be wider and to have a higher saturation than the two adjacent fingers.

In the last case, the source width is $L = 30$, and the simulation result is shown in Figure 7d. Here the flow breaks into four fingers. These fingers first formed at different depths as the infiltrating front moved downward. For this case the tips of the fingers are at a lower saturation, and the saturation within the finger cores is significantly lower than the core saturation observed in the previous cases. The total applied flux of 0.5 is split among the four fingers, but not uniformly. The distribution layer focuses the applied flux to the different fingers in a manner that does not produce an equal partitioning of the flux to the fingers. The position of the fingers are shown at $t = 456$. So for this case the fingers required more than twice the time to reach the depth arrived at in the first case where all of the flux was concentrated into one finger.

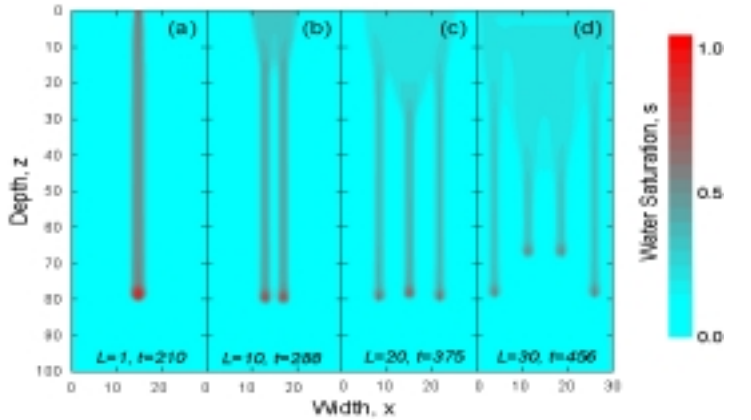

Figure 7 Finger formation as a function of the length, L, of the surface infiltration source for a constant total infiltration across the source surface. The constant infiltration rate $Q = q_0 L = 0.5$ and $n = 7, \tau_s^0 = 5, s_{in} = 0.075$.

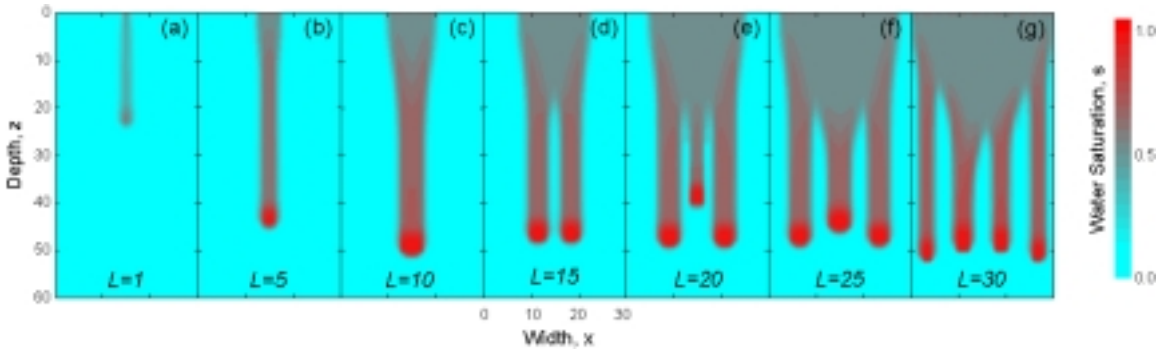

Figure 8 Morphology of the finger flow affected by the length, L, of the infiltration source for the constant intensity $q_0 = 0.2$ and $n = 7, \tau_s^0 = 5, s_{in} = 0.1$. All cases are for the same time $t = 96$.

5.2.2 Constant flux intensity with varying source width

For this set of cases the flux intensity at the soil surface is kept constant while the length of the surface source is varied. The total flux through the soil surface then increases linearly with the length of the source. The saturation distribution within the flow region for the various cases of surface source length is illustrated in Figure 8. All plots are for the same time level equal to $t = 96$.

For the case with $L = 5 (Q = 1.0)$ a distribution layer is present, but the flux through that distribution layer is concentrated entirely into the single finger shown. The higher flux in the finger, five times the flux in the single finger shown in Figure 8a, leads to a much wider finger tip and finger core, and the saturation at the finger tip and within the finger core is also higher. The velocity of the finger propagation is higher as well due to the higher flux within the finger.

The flow distributions resulting from the larger source widths of $L = 10\,(Q = 2.0)$, $L = 15 (Q = 3.0)$, $L = 25 (Q = 5.0)$, and $L = 30 (Q = 6.0)$ are illustrated in Figure 8c through Figure 8g. The simulation results show that as the source width increases, while keeping the surface flux intensity constant, the flow breaks into an increasing number of fingers. There is one finger for $L = 10$, two for $L = 15$, three for $L = 20$, three for $L = 25$, and four for $L = 30$. The fluxes within the individual fingers for each of these cases is approximately Q = 2, Q = 1.5, Q = 1.33, Q = 1.67, and Q = 1.5, respectively. The fingers for all of these cases have width, velocity, and saturation distribution characteristics very similar to those seen in Figure 8b. The small difference in flux within the individual fingers makes them have slightly different width and velocity, but overall the characteristics are very similar. Another aspect of interest here is that the depth of the distribution layer as well as the penetration depth is similar for cases Figure 8c through Figure

8g. This contrasts with the set of runs shown in Figure 7 where the distribution layer thickness increases and the finger penetration depth decreases as the surface flux intensity decreases.

6 Discussion

We observed from the plots in Figure 7 that the distribution layer increases in depth as the surface flux intensity, q_o, decreases. While we have not run extensive tests of the effect of the surface flux intensity, based on the results presented in Figure 7 we hypothesize that as the surface flux intensity decreases toward zero, the depth of the distribution layer will increase without bound. This of course means that the flow will be stable within the scale of the soil profile of interest.

We believe this hypothesis is supported by the experimental results presented by Yao and Hendrickx (1996). They presented experimental results wherein they tested the effect of surface flux intensity on flow instability. They applied surface fluxes in the range from relatively high values, $q_o \simeq 0.01$, to relatively low values $q_o \simeq 0.0001$. The relatively high values correspond to the values used in experiments by previous investigators (e.g., Glass et al., 1989). Yao and Hendrickx showed that for the relatively high fluxes, the flow within the sand columns was unstable, while for the relatively low values the flow was stable. We should note that the flow was apparently stable at the scale of the columns studied by Yao and Hendrickx. Had the columns been larger in diameter or length, perhaps the flow even at these low flux rates might have become unstable at a larger time or space scale.

The idea that flow will be stabilized when the surface flux is relatively small is supported by a rational analysis of the relaxation equation, equation (9). For relatively high fluxes, the $\partial s/\partial t$ term will be significant, and therefore the non-equilibrium will be important and may lead to unstable conditions. In contrast, as the flux decreases the $\partial s/\partial t$ term becomes vanishingly small, leading to the conclusion that $p \simeq \mathrm{P}$, a result that means the flow will be stable. For the numerical results presented in Figure 7d, the applied flux is $q_o \simeq 0.017$. We made a preliminary test of the hypothesis of stabilization of flow at low fluxes by reducing the applied flux by a factor of 10 to $q_o \simeq 0.0017$. For this case the propagating moisture profile was slightly non-monotonic, but within the depth of the profile the flow remained stable.

Relating back to the experiments of Yao and Hendrickx (1996), an intriguing idea that should be considered in future analysis is that even at very low fluxes, it may be possible that within very deep unsaturated zones there would be sufficient distance/time and sufficient disturbances to the flow field for flows to eventually become unstable. The lower flux tested, $q_o \simeq 0.0017$, yielded a slightly non-monotonic profile. Perhaps if the simulation were carried further, the front might become unstable at a larger depth. To study this possibility it will be necessary to develop both analytical solutions as well as numerical simulations of large unsaturated zone systems.

Many of the simulated fingers shown had tips with saturations less than 100%. In most experimental and conceptual descriptions of finger flow the porous media at the tips of fingers are described as being fully saturated. The difference between these experimental and conceptual descriptions and the numerical results presented here may be due to any one or all of the following reasons. First, the parameters for the non-equilibrium model have not been fully determined from experimental data. Until those parameters are determined, it will not be possible to know whether the trends shown in our simulated results are relative or absolute. Second, the initial saturations for our numerical solutions were above residual. In most experimental observations of finger flow the initial saturation is set to the air-dry conditions. One expects to have higher saturations at the advancing front for the drier initial condition. Third, experiments where saturation at the tips of fingers has been measured have been for relatively high surface fluxes. Perhaps experiments with lower surface fluxes would show lower saturations at the tips.

The numerical simulations presented used a specific rational form of equation to represent the relaxation function. We included in that function the dependence of both saturation and pressure. To date only a very small amount of data have been presented in the literature upon which to base an analysis of the saturation and pressure dependence of the relaxation function. The data by Topp et al. (1967) and Wildenschild et al. (2001) were for drainage processes only. Smiles et al. (1973) sought to measure non-equilibrium conditions for wetting processes, in addition to making measurements for drainage processes. The results from all of these studies showed that non-equilibrium is significant for drainage processes, but

Smiles et al. concluded that non-equilibrium is non-existent for the wetting processes they studied. This conclusion conflicts with the imbibition studies of Nielson et al. (1962).

To further study the mathematical nature of unstable flow processes it is essential that much work be done to quantify the degree of non-equilibrium for both wetting and drainage processes, including primary wetting/drainage as well as for secondary wetting/drainage. The horizontal diffusivity experimental technique, like that described by Nielson et al. (1962), in combination with an inverse modeling approach may be useful to derive the relaxation function for wetting processes. To quantify the function for wetting and drying processes it may be best to use pressure cell methods. These are normally operated in a pressure control mode, whereby the pressure is set and the volume of outflow/inflow is measured. A better approach would be to control the rate of outflow/inflow, and measure the pressure. The approach described by Widenschild et al. (2001) where a syringe pump is used to control the flow rate is recommended. With the ever improved accuracy and precision of sensors and instrumentation, in-situ methods in laboratory scale models and in the field may also provide the means to derive the non-equilibrium functions.

Our experience with the numerical solution to equations (1) and (9), as represented by equations (14), has shown that more work needs to be done to improve the ability to handle sharp fronts of saturation and pressure. Adaptive grid refinement methods will need to be adopted to make this improvement. Such improvements in solution efficiency will be necessary before extending the solution to three space dimensions.

7 Conclusions

In this paper we have confirmed the conclusions of Egorov et al. (2002) and Dautov et al. (2002), that solutions of the Richards equation are stable, while the simulation of fingering can be achieved by incorporating both dynamic (relaxation) and static (hysteresis) memory effects into the solution of the equation for mass balance of flow. As shown by Dautov et al., the relaxation mechanism generates fingers while hysteresis leads to the persistence of the fingers. Other mechanisms for finger generation may exist, but these still need to be postulated and examined.

Application of the numerical solution to examine the effect of water repellency on flow instability shows that the sensitivity of the saturation - pressure relationship to the degree of water repellency is sufficient to cause flows to be unstable. Water repellency affects the shape of the wetting curve of the saturation - pressure relationship. The change in shape is described in terms of a flattening of the relationship, and a concurrent increase in the water entry pressure. Even for slight water repellency a porous medium with well-graded particle size distribution can behave like a porous medium with more uniform grading.

Detailed experiments are needed to further quantify the relaxation function adopted in this paper. That function has received significant attention from a theoretical standpoint, but much work remains to derive experimental data. Several approaches can be used to derive these experimental data, including sorptivity methods, volume controlled pressure cell methods, and in-situ laboratory/field methods.

Additional work is needed to improve the numerical methods to solve the governing equations (1) and (9), especially for the case of initially dry media where extremely sharp wetting fronts are involved. Adaptive grid refinement techniques are appropriate to address this issue.

Acknowledgments

The authors wish to acknowledge support under NATO Collaborative Linkage Grant No.978242. Partial support was also provided by the Army High Performance Computing Research Center under the auspices of the Department of the Army, Army Research Laboratory cooperative agreement number DAAD19-01-2-0014, the content of which does not necessarily reflect the position or the policy of the government, and no official endorsement should be inferred.

References

1. Baker, R.S. and D. Hillel, 1990. Laboratory tests of a theory of fingering during infiltration into layered soils, Soil Sci. Soc. Am. J. 54: 20-30.
2. Bauters, T.W.J., DiCarlo, D.A., Steenhuis, T.S., Parlange, J.-Y., 1998. Preferential flow in water-repellent sands. Soil Sci. Soc. Am. J. 62, 1185-1190.

3. Beliaev, A. Y. and S. M. Hassanizadeh, 2001. A theoretical model of hysteresis and dynamic effects in the capillary relation for two-phase flow in porous media, Transp. Porous Med. 43: 487-510.
4. Dautov, R. Z., A. G. Egorov, J. L. Nieber and A. Y. Sheshukov, 2002. Simulation of two-dimensional gravity-driven unstable flow, Proc. 14th Int. Conf. on Comp. Meth. in Wat. Resour. (Delft, The Netherlands) 1: 9-16.
5. de Rooij, G. H., 1995. A three-region analytical model of solute leaching in a soil with a water-repellent top layer. Water Resour. Res. 31: 2701–2707.
6. de Rooij, G. H. and P. de Vries, 1996. Solute leaching in a sandy soil with a water-repellent surface layer: a simulation. Geoderma 70: 253–263.
7. Dekker, L. W. and C. J. Ritsema, 1996. Preferential flow paths in a water repellent clay soil with grass cover. Water Resour. Res. 32: 1239–1249.
8. Diment, G. A., K. K. Watson, and P. J. Blennerhassett, 1982. Stability analysis of water movement in unsaturated porous materials: 1. Theoretical considerations, Water Resour. Res. 18: 1245-1254.
9. Egorov, A. G., R. Z. Dautov, J. L. Nieber and A. Y. Sheshukov, 2002. Stability analysis of traveling wave solution for gravity-driven flow, Proc. 14th Int. Conf. on Comp. Meth. in Wat. Resour. (Delft, The Netherlands) 1: 120-127.
10. Glass, R.J., J.-Y. Parlange, and T.S. Steenhuis, 1989. Wetting front instability, 2. Experimental determination of relationships between system parameters and two-dimensional unstable flow field behavior in initially dry porous media, Water Resour. Res., 25: 1195-1207.
11. Hassanizadeh, S. M., 1997. Dynamic effects in the capillary pressure-saturation relationship, Proc. 4th Int. Conf. on Civil. Eng. (Teheran, Iran) 4: 141-149.
12. Hassanizadeh, S. M. and W. G. Gray, 1993. Thermodynamic basis of capillary pressure in porous media, Water Resour. Res. 29: 3389-3405.
13. Hendrickx, J. M. H., L. W. Dekker, O. H. Boersma, 1993. Unstable wetting fronts in water-repellent field soils, J. Environ. Qual. 22: 109–118.
14. Hill, S., 1952. Channeling in packed columns, Chem. Eng. Sci., 1:247-253.
15. Hill, D. E. and J.-Y. Parlange, 1972. Wetting front instability in layered soils, Soil Sci. Soc. Am. Proc. 36: 697-702.
16. Jamison, V. C., 1945. The penetration of irrigation and rain water into sandy soil of Central Florida, Soil Sci. Soc. Am. Proc. 10: 25-29.
17. Liu, Y., T. S. Steenhuis, and J.-Y. Parlange, 1994. Formation and persistence of fingered flow in coarse grained soils under different moisture contents, J. Hydrol. 159: 187-195.
18. Mualem, Y., 1974. A conceptual model of hysteresis, Water Resour. Res. 10: 514-520.
19. Nguyen, H. V., J. L. Nieber, C. J. Ritsema, L. W. Dekker, and T. S. Steenhuis, 1999. Modeling gravity-driven unstable flow in a water repellent soil, J. Hydrol. 215: 202–214.
20. Nieber, J. L., 1996. Modeling finger development and persistence in initially dry porous media, Geoderma 70: 207-229.
21. Nieber, J. L., 2000. The relation of preferential flow to water quality, and its theoretical and experimental quantification, IN: D. Bosch and K. King (eds.), Preferential Flow, Water Movement and Chemical Transport in the Environment, Proc. of the Second Intern. Symp. on Preferential Flow, Honolulu, Hawaii, Jan. 3-5, 2001, Amer. Soc. Agr. Eng., 1-10.
22. Nieber, J. L., T. W. J. Bauters, T. S. Steenhuis, and J.-Y. Parlange, 2000. Numerical simulation of experimental gravity-driven unstable flow in water repellent sand, J. Hydrol. 231-232: 295-307.
23. Nielson, D. R., G. Biggar and G. Davidson, 1962. Experimental consideration of diffusion analysis in unsaturated flow problems, Soil Sci. Soc. Am. Proc. 26: 107-111.
24. Otto, F., 1997. L^1-contraction and uniqueness for unstationary saturated-unsaturated water flow in porous media, Adv. Math. Sci. Appl. 7: 537-553.
25. Panfilov, M., 1998. Upscaling two-phase flow in double porosity media: Nonuniform homogenization, In: Recent Adv. Prob. Flow Transp. Porous Media, J. M. Crolet and M. E. Hatri (Eds.), 195-215.
26. Parlange, J.-Y. and D. E. Hill, 1976. Theoretical analysis of wetting front instability in soils, Soil. Sci. 122: 236-239.
27. Philip, J. R., 1975. Stability analysis of infiltration, Soil Sci. Soc. Am. Proc., 39: 1042-1049.
28. Raats, P. A. C., 1973. Unstable wetting fronts in uniform and non-uniform soils, Soil Sci. Soc. Am. Proc. 37: 681-685.
29. Ritsema, C. J., L. W. Dekker, J. M. H. Hendrickx and W. Hamminga, 1993. Preferential flow mechanism in a water repellent sandy soil, Water Resour. Res. 29: 2183-2193.

30. Ritsema, C. J. and L.W. Dekker, 1994. How water moves in a water repellent sandy soil, 2. Dynamics of fingered flow, Water Resour. Res. 30: 2519–2531.
31. Ritsema, C. J., L. W. Dekker, J. L. Nieber, and T. S. Steenhuis, 1998. Modeling and field evidence of finger formation and finger recurrence in a water repellent sandy soil, Water Resour. Res. 34: 555–567.
32. Selker, J. S., J.-Y. Parlange and T. Steenhuis, 1992. Fingered flow in two dimensions, 2, Predicting the moisture profile, Water Resour. Res. 28: 2523-2528.
33. Smiles, D. E., G. Vachaud and M. Vauclin, 1971. A test of the uniqueness of the soil moisture characteristic during transient, nonhysteretic flow of water in a rigid soil, Soil Sci. Soc. Am. Proc. 35: 534-539.
34. Topp, G. C., A. Klute and D. B. Peters, 1967. Comparison of water contents-pressure data obtained by equilibrium, steady-state, and unsteady-state methods, Soil Sci. Soc. Am. Proc. 31: 312-314.
35. van Dam, J. C., J. M. H. Hendrickx, H. C. van Ommen, M. H. Bannink, M. T. van Genuchten, and L. W. Dekker, 1990. Water and solute movement in a coarse-textured water-repellent field soil, J. Hydrol. 120: 359–379.
36. van Genuchten, M. T., 1980. A closed form equation for predicting the hydraulic conductivity of unsaturated soil, Soil Sci. Soc. Am. J. 44: 892-898.
37. Wildenschild, D., J. W. Hopmans, and J. Simunek, 2001. Flow Rate Dependence of Soil Hydraulic Characteristics, Soil Sci. Soc. Am. J. 65: 35-48.
38. Yao, T.-M. and J. M. H. Hendrickx, 1996. Stability of wetting fronts in dry homogeneous soils under low infiltration rates, Soil Sci. Soc. Am. J., 60: 20-28.